HHS Public Access

Author manuscript

J Cell Physiol. Author manuscript; available in PMC 2016 March 29.

Published in final edited form as:

J Cell Physiol. 2015 June ; 230(6): 1389–1399. doi:10.1002/jcp.24883.

Phospholipase C Epsilon (PLCε) Induced TRPC6 Activation: A Common but Redundant Mechanism in Primary Podocytes

Hermann Kalwa[1], **Ursula Storch**[2], **Jana Demleitner**[2], **Susanne Fiedler**[2], **Tim Mayer**[2], **Martina Kannler**[2], **Meike Fahlbusch**[2], **Holger Barth**[3], **Alan Smrcka**[4], **Friedhelm Hildebrandt**[5], **Thomas Gudermann**[2], and **Alexander Dietrich**[2,*]

[1]Brigham and Women's Hospital, Harvard Medical School, Boston, Massachusetts

[2]Walther-Straub-Institute of Pharmacology and Toxicology, University of Munich, Munich, Germany

[3]Institute of Pharmacology and Toxicology, University of Ulm Medical Center, Ulm, Germany

[4]Department of Pharmacology and Physiology, University of Rochester, Rochester City, New York

[5]Children's Hospital, Harvard Medical School, Boston, Massachusetts

Abstract

In eukaryotic cells, activation of phospholipase C (PLC)-coupled membrane receptors by hormones leads to an increase in the intracellular Ca^{2+} concentration $[Ca^{2+}]_i$. Catalytic activity of PLCs results in the hydrolysis of phosphatidylinositol 4,5-bisphosphate to generate inositol 1,4,5-trisphosphate (IP3) and diacylglycerol (DAG) which opens DAG-sensitive classical transient receptor channels 3, 6, and 7 (TRPC3/6/7), initiating Ca^{2+} influx from the extracellular space. Patients with focal segmental glomerulosclerosis (FSGS) express gain-of-function mutants of TRPC6, while others carry loss-of-function mutants of PLCε, raising the intriguing possibility that both proteins interact and might work in the same signalling pathway. While TRPC6 activation by PLCβ and PLCγ isozymes was extensively studied, the role of PLCε in TRPC6 activation remains elusive. TRPC6 was co-immunoprecipitated with PLCε in a heterologous overexpression system in HEK293 cells as well as in freshly isolated murine podocytes. Receptor-operated TRPC6 currents in HEK293 cells expressing TRPC6 were reduced by a specific PLCε siRNA and by a PLCε loss-of-function mutant isolated from a patient with FSGS. PLCε-induced TRPC6 activation was also identified in murine embryonic fibroblasts (MEFs) lacking $G\alpha_{q/11}$ proteins. Further analysis of the signal transduction pathway revealed a $G\alpha_{12/13}$ Rho-GEF activation which induced Rho-mediated PLCε stimulation. Therefore, we identified a new pathway for TRPC6 activation by PLCε. PLCε-/- podocytes however, were undistinguishable from WT podocytes in their angiotensin II-induced formation of actin stress fibers and their GTPγS-induced TRPC6 activation, pointing to a redundant role of PLCε-mediated TRPC6 activation at least in podocytes.

[*]Correspondence to: Alexander Dietrich, Walther-Straub-Institute of Pharmacology and Toxicology, Nußbaumstr. 26, 80336 Munich, Germany. Alexander.Dietrich@lrz.uni-muenchen.de.

Hermann Kalwa, Ursula Storch, and Jana Demleitner contributed equally to this work.

Supporting Information: Additional supporting information may be found in the online version of this article at the publisher's web-site.

Receptor-operated Ca^{2+} entry (ROCE) is a fundamental signaling process in all mammalian cells. Transient receptor potential (TRP) channels are regulators of the intracellular Ca^{2+} concentration $[Ca^{2+}]_i$ in many tissues, including vascular smooth muscle, endothelium and kidney. Although the seven members of the classical or canonical TRP family (TRPC1–7) were the first cloned TRP channels in mammals, their functional importance is still poorly understood (Nilius and Owsianik, 2011). Among the TRPC channels, TRPC3, 6, and 7 share 69% identity and are gated by pathways involving receptor stimulated C-type phospholipases (PLCs) and activation by diacylglycerols (DAG) (Rohacs, 2013). Murine TRPC6 cDNA was isolated from brain (Boulay et al., 1997), while human TRPC6 was cloned from placenta (Hofmann et al., 1999). The most prominent expression of TRPC6 however, was found in lung tissues (Boulay et al., 1997). In pulmonary smooth muscle cells TRPC6 is essential for acute hypoxic vasoconstriction (Weissmann et al., 2006) and regulates endothelial permeability inducing lung edema during ischemia-reperfusion injury (Weissmann et al., 2012).

Gain of function mutants of TRPC6 were identified in patients with proteinuria due to inherited forms of focal segmental glomerulosclerosis (FSGS) (Reiser et al., 2005; Winn et al., 2005; Mottl et al., 2013) in their kidney glomeruli. Ultrafiltration of plasma in the glomeruli to dispose of metabolic products, excess electrolytes and water, while retaining blood cells and proteins, is a key function of the kidney glomerulus. The glomerular filter is composed of a fenestrated capillary endothelium, the glomerular basement membrane and podocyte foot processes which are connected by a structure known as the slit diaphragm. In the last years, podocytes have emerged as central players in glomerular research, because podocyte damage weakens the function of the filter and leads to proteinuria, a characteristic feature of most glomerular diseases. For this reason and because podocytes were assumed not to be replaceable, ion channels expressed in glomerular podocytes and their foot processes have attracted special attention and it was hypothesized that the identified TRPC6 mutations may cause FSGS by inducing podocyte dysfunction and cell death. Therefore, channel mutants characterized by increased Ca^{2+} influx (P112Q, [Winn et al., 2005]) or larger current amplitudes (R895C and E897K, [Reiser et al., 2005]) in a heterologous expression system were expressed in immortalized podocyte cell lines. TRPC6 dependent Ca^{2+} influx induced calcineurin activation and synaptopodin dephosphorylation resulting in decreased protection of RhoA, a protein essential for actin polymerization and stress fiber formation, from proteasomal degradation (Faul et al., 2008). Increased levels of TRPC6 expression in cultured podocytes result in a disruption of the actin cytoskeleton and in vivo delivery of cDNA encoding TRPC6 into mice induces proteinuria (Moller et al., 2007). The renin-angiotensin system (RAS) also plays a critical role in modulating proteinuria and progression of glomerulosclerosis (Taal and Brenner, 2000) and TRPC6 channels may represent important effectors in this signal transduction pathway in podocytes. Along these lines, mice lacking TRPC6 (TRPC6-/-) showed significantly less angiotensin II-induced proteinuria compared to wild-type mice (Eckel et al., 2011), indicating that chronic TRPC6 activation is also able to induce FSGS like symptoms.

Moreover, loss of function mutations of phospholipase C epsilon (PLCε) were identified as autosomal recessive determinants in FSGS patients and PLCε is expressed in podocytes

(Hinkes et al., 2006). However, these patients suffer from an early onset of FSGS (Hinkes et al., 2006), while most of the patients with gain of function TRPC6 mutations show a late onset of the disease (Winn et al., 2005). Interestingly, some patients homozygous for PLCε mutations do not show any signs of the disease (Boyer et al., 2010). PLCε enzymes are uniquely regulated by multiple upstream signals including members of the Ras-family and RhoA and generate -like all PLC isozymes- inositol 1,4,5 trisphosphate (IP3) and DAG by cleavage of the phospholipid phosphatidylinositol 4,5, bisphosphate (PIP2) (reviewed in [Smrcka et al., 2012]). These characteristics of PLCε raise the intriguing possibility that increased DAG production after activation of angiotensin receptors by PLCε is able to induce TRPC6 activation in podocytes (Dietrich et al., 2010). In summary, there is evidence for an interaction of both proteins or at least for an important role of both components in the same signaling pathway, while recent clinical data indicate that they might work independently from each other. However, while TRPC6 activation by PLCβ-and PLCγ-isozymes was extensively studied (Rohacs, 2013), the role of PLCε in TRPC activation has never been analysed before (Smrcka et al., 2012). To answer the question if PLCε and TRPC6 are members of the same signal transduction cascade which is disturbed in native podocytes in FSGS patients, we set out to characterize TRPC6-PLCε interaction in different cell types utilising different signalling pathways for TRPC6 activation. We now demonstrate that PLCε co-immunoprecipitates with TRPC6 in a heterologous expression system and lysates from freshly prepared podocytes. We propose a $G\alpha_{12/13}$, RhoGEF-activation resulting in Rho-mediated PLCε stimulation in murine embryonic fibroblasts. Actin stress fiber formation and proliferation however was not altered in PLCε-/- podocytes compared to WT podocytes, while TRPC6-/- podocytes expressed significantly more stress fibres and showed increased proliferation rates. GTPγS induced currents were significantly reduced in TRPC6-/- podocytes, but unaltered in PLCε deficient compared to WT podocytes. Our data indicate an important, but redundant activation of TRPC6 by PLCε which can be replaced by other PLC isoforms.

Materials and Methods

Animals

All animal experiments were approved by the governmental authorities. *TRPC6*-/-, PLCε-/- mice were generated as previously described (Dietrich et al., 2005; Wang et al., 2005).

Isolation of primary podocytes and cell culture of HEK293 cells and murine embryonic fibroblasts (MEFs)

Primary podocytes were isolated from 10 days old pups of the different genotypes essentially as described (Rastaldi et al., 2006) and grown in Dulbecco's modified Eagle medium (DMEM) F12 supplemented with 10% FBS, 5 μg/ml transferrin,10^{-7} M hydrocortisone, 5 ng/ml sodium selenite, 0.12 U/ml insulin, 5 μg/ml normocin (Invivogen, San Diego, CA), 100 μg/ml penicillin, 100 μg/ml streptomycin and 2mM L-glutamine (Sigma–Aldrich, Taufkirchen, Germany). HEK293 cells (DSMZ, Braunschweig, Germany) and murine embryonic fibroblasts (Vogt et al., 2003) were grown in DMEM and 10% FBS. The growth medium of HEK293 cells stably expressing TRPC6-HA was supplemented with 800 μg/ml G418 (Invivogen).

Quantitative RT–PCR analysis

Total RNA from primary podocytes was isolated using an Invitrap® Spin Universal RNA Mini Kit (Invitek, Berlin, Germany). Real time PCR was done using the 2 × Absolute™ QPCR SYBR Green Mix (Thermo Scientific, St. Leon-Rot, Germany). Ten pmol of each primer pair and 0.2 µl from the first strand synthesis were added to the reaction mixture and PCR was carried out in a light-cycler apparatus (Roche, Mannheim, Germany) using the following conditions: 15 min initial activation and 45 cycles of 12 sec at 94 °C, 30 sec at 50 °C, 30 sec at 72 °C. The following primers pairs were used for the amplification of specific PLC DNA-fragments from the first strand synthesis: PLCβ_1, forward (5′-cgcatttctggagaaagcata) and reverse (5′-ccggtctgctgagaacaatc); PLCβ_2 forward (5′-cagtggaccgcattgatgt) and reverse (5′-acaggaactgcccagagatg); PLCβ_3 forward (5′-aaaaagcccaccactgatga) and reverse (5′-acatctcctccgtggcatt); PLCβ_4 forward (5′-ggaggaaagtcttcagtggaaa) and reverse (5′-tcccaacagtcaagttcaaca); PLCγ_1 forward (5′-catgctttcgtagcctcaga) and reverse (5′-tgaagtgctgagccatgttt); PLCγ_2 forward (5′-cggcatcaagtttctcaagg) and reverse (5′-gctgagctcatctttctgtgc); PLCε forward (5′-gggatgtcatctcccatcag) and reverse (5′-ttgcattcctcctcggatt).

Fluorescence intensities were recorded after the extension step at 72 °C after each cycle. Samples containing primer dimers were excluded by melting curve analysis and identification of the products by agarose gel electrophoresis. Crossing points were determined by the software program provided by the manufacturer. Relative gene expression was quantified using the formula: $(2e^{[\text{Crossing point GAPDH - Crossing point} \times]}) \times 100 = \%$ of reference gene expression.

In-vitro mutagenesis

In vitro site-directed mutagenesis has been used to introduce the M131T point mutation in the murine TRPC6 cDNA. Ten pmol of the forward (5′-GTTAACTGTGTGGATTACACGGGCCAGAA TGCCCTACAGC) and the reverse primer (5′-GCTGTAGGGC ATTCTGGCCCGTGTAATCCACACAGTTAAC) containing the mutation have been added to the reaction mixtue (5 × Phusion HF buffer, 10 µl; pcDNA3 plasmid containing the mTRPC6 cDNA, 25 ng; dNTP mix, 10 mM, Phusion HF Polymerase, 2.5 U)(Thermo Scientific, Waltham, MA). PCR was performed using the following conditions: 30 sec initial denaturation and 12 cycles of 30 sec at 95 °C, 1 min at 55 °C, 9 min at 86 °C. Then 1 µl *DpnI* (10 u) was added to the PCR reaction to digest parental methylated and hemimethylated DNA before transformation of E. *coli* DH5α. Plasmid DNA was isolated from single colonies on ampicillin-containing agar plates and sequenced. For incorporation of the TRPC6M131T cDNA into the lentiviral vector pWPXL the insert was released from pcDNA3 by digestion with *BamHI* and *EcoRI* (Thermo Scientific, Waltham, MA) and then ligated into the *BamHI* and *EcoRI* restriction sites of pWPXL.

Co-immuno precipitation

Cells from two cell culture dishes were washed with PBS and 2 ml of lysis buffer (20 mM Tris-HCL, pH 7.5, 150 mM NaCl, 1% Nonidet P40, 0.5% sodium deoxycholate, 1% SDS, 5 mM EDTA) was applied for 30 min at 4 °C. Proteins were homogenized, 200 ng of antibody

(GFP ab.: Takara Bio Europe SAS, Saint-Germain-en-Laye, France, #632377; Hemagglutinin ab.: Sigma, Taufkirchen, Germany, #H6903; IgG from mouse serum: Sigma, Taufkirchen, Germany, #I5381; PLCβ1 ab.: Sigma, Taufkirchen, Germany, #SAB2104946; PLCε ab.: Santa Cruz Biotechnology Inc., Heidelberg, Germany, sc-28404) was applied overnight, incubated with 30 µl of protein A-sepharose for 2 h and centrifuged at 4 °C After centrifugation at 5500 × g for 3 min at 4 °C sepharose-bound proteins were washed three times in lysis buffer, resuspended in 40 µl Laemmli buffer, incubated at 90 °C for 10 min and analyzed by immunoblotting.

Immunoblotting

After heating to 90 °C for 10 min and sonication for 15 sec, 20µl of each sample was loaded on a 10% SDS gel. Protein separation was performed at room temperature using a current of 20 mAmp for 2–3 h. To transfer the proteins to a PVDF membrane a current of 20 mAmp was applied for 20 h at 4°C. After transfer, PVDF membrane was rinsed with 10 ml PBST for 5 min at room temperature. Transfer was checked using Ponceau solution (A2935 0500, AppliChem, Darmstadt, Germany). Blocking was performed for 1 hat room temperature using 10 ml blocking buffer (5% low fat milk in PBST). Each primary antibody was diluted in PBST containing 0.05% sodium azide according manufacturer's protocol and applied over night at 4 °C. After washing with PBST three times for 10 min each, HRP-conjugated secondary antibody was applied for 2 h at room temperature. After incubation the membrane was washed with PBST once more for three times, 10 minutes each. Detection was made using Super Signal West Dura chemiluminescent substrate (34075, Thermo Scientific Waltham, MA) and Carestream BioMax Light films (8194540, Kodak, Rochester, NY) or chemi-smart (Peqlab, Erlangen, Germany). Used antibodies and dilutions were: HRP-conjugated anti β-actin antibody (Sigma A3854HRP, 1:10,000); anti CD144 antibody (rabbit, Cell Signaling #2500, 1:1000) and secondary antibody anti rabbit-HRP (Sigma A6154, 1: 10000); anti HA antibody (rat, Roche 11867423001, 1:1000) and secondary antibody anti rat-HRP (Sigma A-5795, 1: 1.000); anti nephrin antibody (guinea pig, Acris BP5030, 1:500) and secondary antibody anti guinea pig-HRP (Acris R1322HRP, 1: 2.000); anti podocin antibody (rabbit, Sigma P0372, 1:1000) and secondary antibody anti rabbit-HRP (Sigma A6154, 1: 10,000); anti synaptopodin antibody (mouse, Acris BM5086, 1:10) and secondary antibody anti mouse-HRP (Cell Signaling#7076, 1: 2000); anti TRPC6 antibody (rabbit, Alomone ACC120, 1:200) and secondary antibody anti rabbit-HRP (Sigma A6154, 1: 10,000); anti vinculin antibody (mouse, Sigma V9131, 1:10,000) and secondary antibody anti mouse-HRP (Cell Signaling #7076, 1: 2000); anti WT1 antibody (rabbit, Santa Cruz, sc-192, 1:200) and secondary antibody anti rabbit-HRP (Santa Cruz, sc-2004, 1:5000); anti $PLC\beta_1$ antibody (rabbit, Sigma SAB2104946, 1:1000) and secondary antibody anti rabbit-HRP (Sigma A6154, 1: 10,000); anti PLCε antibody (rabbit, Santa Cruz, sc-368392, 1:300) and secondary antibody anti rabbit-HRP (Santa Cruz, sc-2004, 1:5000).

Immunofluorescence

Cells were seeded on 18 × 18 mm cover slips. For fixation cells were washed three times with PBS and incubated in 3.7% formaldehyde for 15 min at room temperature. After fixation, formaldehyde was removed by rinsing with PBS for three times. Blocking and permeabilization was performed for 1 h at room temperature using a mixture of 5% goat

serum, 0.3% Triton X-100 and PBS. All antibodies were diluted in blocking buffer according manufacturer's protocol. Primary antibody was incubated overnight at 4 °C After rinsing three times with PBS for 5 min each, secondary antibody was applied for 2 h. Samples were washed again three times with PBS for 5 min each. To counterstain cell nuclei an additional staining with Hoechst 33342 (Life Technologies, Darmstadt, Germany) was applied. Used antibodies and dilutions were: anti α-smooth muscle actin (α-SMA) antibody (mouse, Sigma A2547, 1:400) and secondary antibody anti mouse-FITC (Sigma F9006-FITC, 1: 1.000); anti CD144 antibody (rabbit, Cell Signaling #2500, 1:400) and secondary antibody anti rabbit-Alexa488 (Life Technologies, Darmstadt, Germany A11008 Alexa 488, 1:1000); anti nephrin antibody (guinea pig, Acris BP5030, 1:50) and secondary antibody anti guinea pig-Alexa488 (Sigma F6261Alexa488, 1:80); anti podocin antibody (rabbit, Sigma P0372, 1:100) and secondary antibody anti rabbit-Alexa488 (Life Technologies, Darmstadt, Germany, A11008 Alexa 488, 1:1000); anti synaptopodin antibody (mouse, Acris BM5086, undiluted) and secondary antibody anti mouse-FITC (Sigma F9006-ITC, 1: 1.000); anti WT1 antibody (rabbit, Santa Cruz, sc-192, 1:50) and secondary antibody anti rabbit-Alexa488 (Life Technologies, Darmstadt, Germany, A11008 Alexa 488, 1:1000).

Inhibition of Rho proteins by ADP-ribosylating enzymes

The ADP-ribosylating toxins C2I and C2INC3 (each 200 ng/ml medium) were applied together with the transport protein C2IIa (400 ng/ml medium) to murine embryonic fibroblasts (MEF) as described (Barth et al., 1998; Barth and Stiles, 2008). C2I induces an irreversible break down of the actin cytoskeleton with cell apoptosis after 12–24 h and serve as a control, while C2INC3 specifically ADP ribosylates Rho A, B, and –C in between 3 h. Cells were analyzed for LPA-induced increases in $[Ca^{2+}]_i$ 3 h after incubation.

Cell Proliferation by EdU incorporation

5-ethynyl-2′-deoxyuridine (EdU) labeling is a method similar to *5-bromo-2′-deoxyuridine* (BrdU) labeling but with increased reproducibility as well as decreased assay time and loss of *enzymatic disruption of helical DNA structure*. EdU is a thymidine analogue which gets incorporated into DNA during active DNA synthesis, if added to the culture medium. After incorporation the ethynyl group of EdU covalently couples to a small fluorescent azide in a copper-dependent click reaction, which can be detected under a fluorescence microscope (Buck et al., 2008).

EdU was added to culture medium of cells growing on coverslips, to reach a concentration of 10 μM, followed by incubation for 24 h at 37 °C and 5% CO_2 in a common incubator. After fixation and permeabilization using methanol, a blocking solution containing 3% BSA/PBS was added for 1 h. Following this, the coverslips were incubated under exclusion of light for 30 min at room temperature with the click-it reaction cocktail, consisting of 10 μl 1 M Tris/HCl buffer pH7, 4μl 100 mM $CuSO_4$, 5 μl 1M sodium ascorbate, 0.2μl 10 mM azide dye (Baseclick GmbH, Tutzing, Germany) and 80 μl H_2O. To detect all cell nuclei, an additional staining with Hoechst 33342 (Life Technologies, Darmstadt, Germany) was performed.

Phalloidin staining of actin stress fibers

Polymerized actin filaments were stained with Alexa Fluor Phalloidin (Life Technologies, Darmstadt, Germany) according to manufactures protocols. To counterstain cell nuclei an additional incubation with Hoechst 33342 (Life Technologies) was performed. Sample preparation and visualization was carried out as described in the previous paragraph.

SiRNA and shRNA transfections

Mouse embryonic fibroblasts (MEFs) were seeded and grown to 70–80% confluency in six-well plates. PLCε siRNA constructs (Silencer®Select), Pre-designed siRNAs (from ambion® by Life technologies, Darmstadt, Germany); sense, GCA UUG UCU UCG ACG ACA A, antisense UUG UCG UCG AAG ACA AUG C;) and control siRNA (sense, UAA CGA CGC GAC GAC GUA A, antisense UUA CGU CGU CGC GUC GUU A) labelled with Alexa fluor 648 dye were transfected with the lipofectamine®2000 reagent (Life technologies, Darmstadt, Germany). HEK293 cells expressing TRPC6 were seeded and grown to 70–80% confluency in six-well-plates. PLCβ1 siRNA (ON TARGET plus, smart pool, L-010280–00-0005, Dharmacon, GE Healthcare, Munich, Germany) or control siRNA (ON TARGET plus, Nontargeting pool, D-001810-10–05, Dharmacon, GE Healthcare) were transfected with lipofectamine®2000 reagent (Life technologies), respectively.

Cells were transfected under serum-free (Opti-Mem®; Life Technologies) conditions with a final concentration of 100 nm siRNA according to the manufactor's protocol. Five hours after transfection the cells were switched into a cell growth medium (DMEM; Lonza, Cologne, Germany) and were incubated for another 48 h. Cells were lysed with lysis buffer and RNA was isolated using spin columns (InviTrap®Spin Universal RNA Mini Kit, Stratec Molecular GmbH, Berlin, Germany) and quantitative RT-PCR was performed as described above. The following oligos were ligated into the *Bgl*II and *HindI*II sites of the pSUPER vector: sense, GAT CCC CAG CCG ATG GCA GTT TAT AAT TCA AGA GA T TAT AAA CTG CCA TCG GCT TTT TTG GAA A; antisense, AGC TTT TCC AAA AAA GCC GAT GGC AGT TTA TAA TCT CTT GAA TTA TAA ACT GCC ATC GGC TGG G. The resulting vector was transfected in HEK293 cells by using the lipofectamin reagent as described above to produce shRNAs after transcription.

Electrophysiology

Performing patch-clamp measurements in the whole cell configuration cation currents were analyzed in HEK293 cells transiently expressing TRPC6 or TRPC6M131T and muscarinic M5 receptor and in WT, PLCε-/- and TRPC6-/- podocytes. For podocytes measurements cation current increases were induced by infusions of 500 μM GTPγS, a nonhydrolizable GTP analogue, through the patch pipette the whole cell mode or by application of 50 μM flufenamate in the bath solution. Basal currents were determined at the beginning of the measurements after patch rupture, maximal GTPγS induced currents were determined after 3 min. For HEK293 measurements maximal currents before and during agonist stimulation with carbachol and during application of the TRPC6 activator flufenamate were used for analysis. In a cell culture dish mounted to a small perfusion chamber adherent podocytes were superfused with the extracellular solution (in mM): NaCl 140, CsCl 5, $CaCl_2$ 2, $MgCl_2$ 1, glucose 10, HEPES 10, adjusted to pH 7.4 with NaOH. Chloride channel blockers 5-

nitro-2-(4-phenylpropylamino) benzoic acid (NPBB, 50 μM) and disodium 4,4′-diisothiocyanatostilbene-2,2′-disulfonate (DIDS, 300 μM) were added to the extracellular solution to block endogenous chloride channels in podocytes. Data were acquired at a frequency of 5 kHz after filtering at 1.67 kHz with an EPC10 patch clamp amplifier (HEKA, Lambrecht, Germany) using the Patchmaster 2.73 software (HEKA). Patch pipettes of resistances of 2.5 to 3.5 MΩ caused series resistances of 6 to 11 MΩ. Patch electrodes were filled with intracellular solution (in mM: CsCl 120, NaCl 9.4, $MgCl_2$ 1 and $CaCl_2$ 3.949 buffered at 100 nM free Ca^{2+} with 10 mM BAPTA and 10 mM HEPES titrated to pH 7.2 with CsOH). The liquid junction potential was +4.0 mV and offset corrections were made by the Patchmaster software. The osmolarity of all solutions was 300 ± 5 mOsm kg^{-1} measured using the vapor osmometer Vapro 5520 (Wescor, Logan Utah (UT), USA). Podocytes were held at a potential of −60 mV, and current–voltage relations were obtained from triangular voltage ramps from −100 to +60 mV with a slope of 0.4 V s^{-1} applied at a frequency of 1 Hz. Experiments were performed at room temperature.

Results

We used co-immunoprecipitation to identify physical interactions of TRPC6 and PLCε expressed in a heterologous expression system. To this end, HEK293 cells stably expressing hemagglutinin-tagged human TRPC6 (HEK TRPC6-HA) were transfected with cDNAs coding for PLCβ and PLCε isoforms (Fig. 1A, see Supplementary Fig. 1A for transfection efficency). TRPC6-HA was co-immunoprecipitated only with specific anti-hemagglutinin and anti-PLCε antibodies from HEK293 cells heterologously expressing PLCε, but not with immunoglobulin γ and antibodies directed against the green fluorescent protein (GFP) and PLCβ (Fig.1B). Vice versa PLCε was co-immunoprecipitated with TRPC6-HA using anti-hemagglutinin antibodies (Supplementary Fig. 1B). Native expression of PLCε in HEK293 cells was not sufficient to detect co-immunoprecipitation of TRPC6 and PLCε (see Fig. 1B). To assess PLCε and TRPC6 interaction in a functional assay, we characterized TRPC6 currents in HEK293 cells by analysis of cationic currents performing whole-cell patch clamp recordings. After heterologous expression of muscarinic acetylcholine receptor 5 (M5) and TRPC6 in HEK293 cells receptor activation by carbachol or the addition of the TRPC6 activator flufenamate (Jung et al., 2002) induced a characteristic double rectifying TRPC6 current as described before ([Dietrich et al., 2003], see Fig. 2B), while in non-transfected HEK293 cells both drugs did not induce any currents differing from currents obtained under basal conditions (see Fig. 2A). In similar transfected cells additionally expressing scrambled control shRNAs carbachol (CCh) activation gave rise to the same rapidly developing transient outward and inward currents (Fig. 2C, E). A similar but significantly reduced current (Fig. 2D, E) was detected in transfected HEK293 cells expressing PLCε-specific shRNAs confirming an important role of PLCε-induced TRPC6 activation at least in a heterologous expression system (summarized in Fig. 2E). As expected, $PLC\beta_1$ mediated activation of TRPC6 is also inhibited by a $PLC\beta_1$ specific siRNA but not by the siRNA control (see Fig. 2 F–H and for specificities of used shRNAs and siRNAs please refer to Supplementary Fig. 1C and D). As down-regulation of both PLC isoforms results in ∼50% current inhibition they are not able to compensate for each other.

Along these lines, expression of a PLCε loss-of-function mutant from a patient with severe proteinuria (Hinkes et al., 2006) in HEK293 cells heterologously expressing M5 and TRPC6 induced significantly decreased currents compared to cells expressing wild-type PLCε (Fig. 3A, B, D). To gain more insight into possible activation mechanisms of PLCε, we deleted the Ras binding sites RA1 and RA2 of PLCε (Bunney et al., 2006), but found no differences to HEK293 cells transfected with PLCε WT and heterologously expressing M5 and TRPC6 (Fig. 3 A, C, D and see Supplementary Fig. 1 F for protein expression of PLCε mutants).

To dissect pathways for PLCε activation we utilized MEFs and activated LPA receptors coupling to both G$\alpha_{q/11}$- and G$\alpha_{12/13}$-dependent pathways. As illustrated in Figure 4 application of lysophosphatic acid (LPA) resulted in an increase in $[Ca^{2+}]_i$ levels in wild-type (WT) cells, which was slightly but not significantly increased by heterologously expressed TRPC6 channels (Fig. 4A). MEFs deficient of G$\alpha_{q/11}$ (Fig. 4B) or G$\alpha_{12/13}$ proteins (Fig. 4C) reacted with significantly smaller changes in $[Ca^{2+}]_i$ with lowest levels detected in G$\alpha_{q/11}$-/- MEFs confirming the assumption that most of the Ca^{2+} influx through TRPC channels is induced by the G$\alpha_{q/11}$ pathway (Vogt et al., 2003). While expression of TRPC6 channels in WT and G$\alpha_{12/13}$ deficient MEFs did not result in a significantly higher increase in LPA-induced $[Ca^{2+}]_i$ (Fig. 4A, C, D), heterologously expressed TRPC6 induced higher increases of $[Ca^{2+}]$i in G$\alpha_{q/11}$ deficient MEF than in G$\alpha_{q/11}$ deficient MEFs expressing only native TRPC (Fig 4B, D). These LPA-induced increases in $[Ca^{2+}]$i in G$\alpha_{q/1}$1 deficient MEFs expressing TRPC6, however, were inhibited in cells transfected with siRNAs specific for PLCε in contrast to cells transfected with the scrambled control siRNA (Fig. 4E). Specificities of PLCε siRNAs were tested in quantitative RT-PCR experiments in MEFs (Supplementary Fig. 1D) resulting in an mRNA down-regulation of 79.82 ± 2% 48 h after transfection. Next, we sought to gain deeper insight into possible activation mechanisms of PLCε through Rho-inhibition by the specific ADP-ribosylating enzyme C2INC3, because RhoA is another potent activator of PLCε (Seifert et al., 2004). Most interestingly, ADP-ribosylation of Rho inhibited LPA-induced $[Ca^{2+}]_i$ increases in G$\alpha_{q/11}$ deficient MEF expressing TRPC6, while the C2I enzyme evoking an irreversible break-down of the actin cytoskeleton was ineffective (Fig. 4F). These data point to a G$\alpha_{12/13}$ Rho-GEF induced RhoA activation of PLCε resulting in the activation of heterologously expressed TRPC6 channels in G$\alpha_{q/11}$ deficient MEFs (summarized in Fig. 4G). However, in G$\alpha_{12/13}$ deficient MEFs TRPC6 activation by PLCβ_1 was at least 2.5 times higher than by PLCε in G$\alpha_{q/11}$ deficient MEF.

To evaluate the identified TRPC6 PLCε interaction in native cells and to assess its importance for FSGS, freshly isolated primary podocytes were prepared as described in *Materials and Methods* and identified by their expression of nephrin, podocin, WT1 and synaptopodin protein analyzed in immunohistochemical and immunoblotting experiments by specific antibodies (Fig. 5A, B and Supplementary Fig. 3). A PLCε antibody recognizing PLCε in primary podocytes (Supplementary Fig. 1G) was able to co-immunoprecipitate TRPC6 from lysates of podocytes (Fig. 5C) and kidney cortex (Fig. 5D). To identify pathways dependent on both TRPC6 and PLCε we tried to heterologously express TRPC6 WT and TRPC6 M131T proteins in WT and TRPC6-/- primary podocytes using recombinant lentiviruses. However expression of TRPC6 proteins in both cell types resulted

in immediate cell death for unknown reasons (see Supplementary Fig. 4). Therefore, we further analyzed podocytes from different genotypes. Most interestingly TRPC6-/- podocytes showed significantly more actin stress fibers than WT and PLCε-/- podocytes (Fig. 6A, B). Moreover, after adding angiotensin II (AngII), no significant increase in stress fiber formation was detected in TRPC6-deficient podocytes, while WT and PLCε-deficient podocytes formed significantly more fibers (Fig. 6A, B). DNA-synthesis was quantified as a marker for cell proliferation of podocytes. Again, WT and PLCε-/- podocytes had similar proliferation rates, while TRPC6-/-podocytes showed increased DNA-synthesis (Fig. 6C). To activate all G protein coupled signaling pathways in primary podocytes and to evaluate the role of PLCε-induced TRPC6 activation in these transduction cascades, we analyzed GTPγS- and flufenamate-induced currents in primary podocytes and detected no differences in current densities of PLCε-/- compared to WT-podocytes, while TRPC6-/- podocytes showed significantly decreased currents (Fig. 6D, E, F, G). The fact that currents induced by GTPγS and by the TRPC6 activator flufenamate (Jung et al., 2002) were similar and absent in TRPC6-/- cells clearly indicate that we are able to identify native TRPC6 currents in primary podocytes.

Because other PLC isoforms may be up-regulated in PLCε-/- podocytes, we quantified PLC mRNA expression in WT, TRPC6-/- and PLCε-/- podocytes. mRNA expression of PLC isoforms was not increased in PLCε-/- podocytes compared to WT-cells (see Supplementary figure 2) but rather decreased in PLCε-/- podocytes. A significant up-regulation of PLCβ_2 mRNA was only detected in TRPC6-/- podocytes.

Discussion

Mutations in the TRPC6 channel (reviewed in [Mottl et al., 2013]) as well as in the PLCε isoform (Hinkes et al., 2006) were detected in patients with FSGS raising the intriguing possibility that both proteins are obligatory for the same signal transduction cascade in native podocytes and that changed protein activities are responsible for the characteristic phenotype of the disease. Therefore, we set out to analyze physical and functional interactions of TRPC6 and PLCε in different cell types and signaling pathways.

We were able to co-immunoprecipitate TRPC6 in a heterologous expression system and in podocytes (Figs. 1 and 5, panel C and D). Moreover, PLCε-mediated DAG production is able to activate TRPC6, if a G$\alpha_{q/11}$-mediated pathway inducing PLCβ activation is deleted. This conclusion is based on a more than 10-fold increase in LPA-induced elevation of $[Ca^{2+}]_i$ in G$\alpha_{q/11}$-/- MEFs expressing TRPC6, which is blocked by a specific PLCε siRNA or Rho-inhibiting toxin (Fig. 4). Because the LPA receptor is coupling to both $G_{q/11}$ and $G_{12/13}$ proteins (reviewed in [Wettschureck and Offermanns, 2005]), we propose a G$\alpha_{12/13}$-mediated Rho-GEF activation of RhoA, which induces DAG production by the PLCε isoform in G$\alpha_{q/11}$-/- MEFs. Most interestingly and in contrast to MEFs, a PLCε-mediated TRPC6-activation is detectable in carbachol-stimulated HEK293 cells stably expressing TRPC6 through its inhibition by an FSGS-specific PLCε loss-of-function-mutant and by specific PLCε shRNAs (Fig. 2, 3). Moreover a murine homologue of a gain-of-function mutant of TRPC6 (TRPC6M131T, [Heeringa et al., 2009]) identified in FSGS patients is also activated by PLCε (Fig 3, panel H–J). As carbachol activation of muscarinic

acetylcholine receptors results only in $G_{q/11}$ activation (reviewed in [Wettschureck and Offermanns, 2005]), a $G\alpha_{q/11}$ induced p63RhoGEF-activation of RhoA (Lutz et al., 2005) seems to be more important in PLCε-induced TRPC6 activation in this cell type. Activation of TRPC6 by PLCε however was only detectable in a HEK293 cell line overexpressing TRPC6 or in a MEF cell line with deleted $G\alpha_{q/11}$ proteins (Fig. 4).

To finally evaluate TRPC6-PLCε interaction in native podocytes we freshly isolated primary podocytes from mice of different genotypes, because it is indispensable to analyze the proteins in their native environment and not only in cell lines or in heterologous expression systems. PLCε-deficiency in native podocytes revealed no significant differences in DNA synthesis as a marker for cell proliferation and actin stress fiber formation. To activate all possible G protein-regulated pathways in native podocytes, we used GTPγS and analyzed currents by the patch clamp technology. Current densities in PLCε-deficient cells analyzed by patch clamp recordings before and after application of GTPγS were indistinguishable to WT cells, but were decreased in TRPC6-/- cells. Most interestingly, the loss of current densities in TRPC6-/- cells as well as the induction of currents in WT and PLCε-/- cells by the TRPC6 activator flufenamate (Jung et al., 2002) which were similar to currents induced by GTPγS clearly indicate that we were able to identify native TRPC6 currents in primary podocytes. These data highlight the importance of TRPC6 channels for native podocyte function as it was also demonstrated in three recent manuscripts characterizing TRPC6-like currents in rat podocytes attached to glomerular capillaries (Roshanravan and Dryer, 2014; Anderson et al., 2014) and in freshly isolated murine podocytes (Ilatovskaya et al., 2014). However, PLCε-deficient podocytes do not resemble characteristics of TRPC6-/- podocytes. Therefore, it seems unlikely that PLCε is indispensable for TRPC6 activation in primary podocytes and if lost, induces FSGS in patients.

These data are in line with the identification of PLCε loss of function mutation in a larger number of patients with diffuse mesangial sclerosis (DMS) (7 patients) rather than with FSGS (2 patients) (Hinkes et al., 2006). Only one additional patient was identified with both histological pathologies. Moreover, no apparent FSGS phenotype was found in PLCε-/- mice and only a PLCε_1 knockdown in the zebra fish model resembled a phenotype similar to human nephrotic syndrome (Hinkes et al., 2006). Along these lines, homozygous or heterozygous PLCε_1 mutations were identified in 33% of analyzed DMS patients but only in 8% of FSGS patients (Boyer et al., 2010). Most interestingly, the latter study also identified three unaffected individuals with homozygous PLCε mutations (Boyer et al., 2010), pointing to other modifier genes and environmental factors which may explain the renal phenotype variability in individuals bearing PLCε mutations. Moreover, in all patients with TRPC6 gain of function except one ([Heeringa et al., 2009] and reviewed in Mottl et al., 2013) a late onset of FSGS was observed, while patients with PLCε mutations suffer from FSGS early in their life.

Soon after cloning the first TRPC genes, PLCβ and PLCγ isoforms were exclusively made responsible for opening TRPC channels after activation of G protein- (Boulay et al., 1997) or tyrosine kinase-coupled (Li et al., 1999) receptors, respectively. Moreover, in podocytes PLCβ isoforms are essential for angiotensin II-mediated activation of TRPC6 (reviewed in [Gudermann, 2005]) and PLCγ1 seems to be important for translocation of TRPC6 to the

plasma membrane (Kanda et al., 2011). We now present evidence for a PLCε-TRPC6 interaction in a heterologous expression system with over-expressed TRPC6 and PLCε proteins and in native podocytes. Moreover, PLCε-mediated DAG production is able to activate TRPC6, if a $G\alpha_{q/11}$-mediated pathway inducing PLCβ activation is deleted. However, this signaling mechanism appears to be masked by PLCβ activity, because these isoforms display at least 20 times higher expression levels in native cells including podocytes (see Supplementary Fig. 2) compared to PLCε. Therefore, PLCε maybe essential for other cellular processes in native podocytes, but activation of TRPC6 is only an important alternative signal transduction pathway in cells expressing TRPC6, if the $G\alpha_{q/11}$-PLCβ pathway is blocked.

Supplementary Material

Refer to Web version on PubMed Central for supplementary material.

Acknowledgments

We would like to thank Christiana Oehlmann and Brigitte Mayerhofer for excellent technical assistance and Dr. Stefan Offermanns (MPI, Bad Nauheim) for his generous gift of $G\alpha_{q/11}$ deficient and $G\alpha_{12/13}$ deficient MEFs. This work was funded by the Fritz-Thyssen-Stiftung.

Contract grant sponsor: Fritz-Thyssen-Stiftung.

Literature Cited

Anderson M, Roshanravan H, Khine J, Dryer SE. Angiotensin II activation of TRPC6 channels in rat podocytes requires generation of reactive oxygen species. J Cell Physiol. 2014; 229:434–442. [PubMed: 24037962]

Barth H, Hofmann F, Olenik C, Just I, Aktories K. The N-terminal part of the enzyme component (C2I) of the binary Clostridium botulinum C2 toxin interacts with the binding component C2II and functions as a carrier system for a Rho ADP-ribosylating C3-like fusion toxin. Infect Immun. 1998; 66:1364–1369. [PubMed: 9529054]

Barth H, Stiles BG. Binary actin-ADP-ribosylating toxins and their use as molecular Trojan horses for drug delivery into eukaryotic cells. Curr Med Chem. 2008; 15:459–469. [PubMed: 18289001]

Boulay G, Zhu X, Peyton M, Jiang M, Hurst R, Stefani E, Birnbaumer L. Cloning and expression of a novel mammalian homolog of Drosophila transient receptor potential (Trp) involved in calcium entry secondary to activation of receptors coupled by the Gq class of G protein. J Biol Chem. 1997; 272:29672–29680. [PubMed: 9368034]

Boyer O, Benoit G, Gribouval O, Nevo F, Pawtowski A, Bilge I, Bircan Z, Deschenes G, Guay-Woodford LM, Hall M, Macher MA, Soulami K, Stefanidis CJ, Weiss R, Loirat C, Gubler MC, Antignac C. Mutational analysis of the PLCE1 gene in steroid resistant nephrotic syndrome. J Med Genet. 2010; 47:445–452. [PubMed: 20591883]

Buck SB, Bradford J, Gee KR, Agnew BJ, Clarke ST, Salic A. Detection of S-phase cell cycle progression using 5-ethynyl-2′-deoxyuridine incorporation with click chemistry, an alternative to using 5-bromo-2′-deoxyuridine antibodies. BioTechniques. 2008; 44:927–929. [PubMed: 18533904]

Bunney TD, Harris R, Gandarillas NL, Josephs MB, Roe SM, Sorli SC, Paterson HF, Rodrigues-Lima F, Esposito D, Ponting CP, Gierschik P, Pearl LH, Driscoll PC, Katan M. Structural and mechanistic insights into ras association domains of phospholipase C epsilon. Mol Cell. 2006; 21:495–507. [PubMed: 16483931]

Dietrich A, Chubanov V, Gudermann T. Renal TRPathies. J Am Soc Nephrol. 2010; 21:736–744. [PubMed: 20395377]

Dietrich A, Mederos YSM, Gollasch M, Gross V, Storch U, Dubrovska G, Obst M, Yildirim E, Salanova B, Kalwa H, Essin K, Pinkenburg O, Luft FC, Gudermann T, Birnbaumer L. Increased vascular smooth muscle contractility in TRPC6-/- mice. Mol Cell Biol. 2005; 25:6980–6989. [PubMed: 16055711]

Dietrich A, Mederos y, Schnitzler M, Emmel J, Kalwa H, Hofmann T, Gudermann T. N-linked protein glycosylation is a major determinant for basal TRPC3 and TRPC6 channel activity. J Biol Chem. 2003; 278:47842–47852. [PubMed: 12970363]

Eckel J, Lavin PJ, Finch EA, Mukerji N, Burch J, Gbadegesin R, Wu G, Bowling B, Byrd A, Hall G, Sparks M, Zhang ZS, Homstad A, Barisoni L, Birbaumer L, Rosenberg P, Winn MP. TRPC6 enhances angiotensin II-induced albuminuria. J Am Soc Nephrol. 2011; 22:526–535. [PubMed: 21258036]

Faul C, Donnelly M, Merscher-Gomez S, Chang YH, Franz S, Delfgaauw J, Chang JM, Choi HY, Campbell KN, Kim K, Reiser J, Mundel P. The actin cytoskeleton of kidney podocytes is a direct target of the antiproteinuric effect of cyclosporine A. Nat Med. 2008; 14:931–938. [PubMed: 18724379]

Gudermann T. A new TRP to kidney disease. Nat Genet. 2005; 37:663–664. [PubMed: 15990884]

Heeringa SF, Moller CC, Du J, Yue L, Hinkes B, Chernin G, Vlangos CN, Hoyer PF, Reiser J, Hildebrandt F. A novel TRPC6 mutation that causes childhood FSGS. PLoS One. 2009; 4:e7771. [PubMed: 19936226]

Hinkes B, Wiggins RC, Gbadegesin R, Vlangos CN, Seelow D, Nurnberg G, Garg P, Verma R, Chaib H, Hoskins BE, Ashraf S, Becker C, Hennies HC, Goyal M, Wharram BL, Schachter AD, Mudumana S, Drummond I, Kerjaschki D, Waldherr R, Dietrich A, Ozaltin F, Bakkaloglu A, Cleper R, Basel-Vanagaite L, Pohl M, Griebel M, Tsygin AN, Soylu A, Muller D, Sorli CS, Bunney TD, Katan M, Liu J, Attanasio M, O'Toole JF, Hasselbacher K, Mucha B, Otto EA, Airik R, Kispert A, Kelley GG, Smrcka AV, Gudermann T, Holzman LB, Nurnberg P, Hildebrandt F. Positional cloning uncovers mutations in PLCE1 responsible for a nephrotic syndrome variant that may be reversible. Nat Genet. 2006; 38:1397–1405. [PubMed: 17086182]

Hofmann T, Obukhov AG, Schaefer M, Harteneck C, Gudermann T, Schultz G. Direct activation of human TRPC6 and TRPC3 channels by diacylglycerol. Nature. 1999; 397:259–263. [PubMed: 9930701]

Ilatovskaya DV, Palygin O, Chubinskiy-Nadezhdin V, Negulyaev YA, Ma R, Birnbaumer L, Staruschenko A. Angiotensin II has acute effects on TRPC6 channels in podocytes of freshly isolated glomeruli. Kidney Int. 2014; 86:506–514. [PubMed: 24646854]

Jung S, Strotmann R, Schultz G, Plant TD. TRPC6 is a candidate channel involved in receptor-stimulated cation currents in A7r5 smooth muscle cells. Am J Physiol Cell Physiol. 2002; 282:C347–359. [PubMed: 11788346]

Kanda S, Harita Y, Shibagaki Y, Sekine T, Igarashi T, Inoue T, Hattori S. Tyrosine phosphorylation-dependent activation of TRPC6 regulated by PLC-gamma1 and nephrin: Effect of mutations associated with focal segmental glomerulosclerosis. Mol Biol Cell. 2011; 22:1824–1835. [PubMed: 21471003]

Li HS, Xu XZ, Montell C. Activation of a TRPC3-dependent cation current through the neurotrophin BDNF. Neuron. 1999; 24:261–273. [PubMed: 10677043]

Lutz S, Freichel-Blomquist A, Yang Y, Rumenapp U, Jakobs KH, Schmidt M, Wieland T. The guanine nucleotide exchange factor p63RhoGEF, a specific link between Gq/11-coupled receptor signaling and RhoA. J Biol Chem. 2005; 280:11134–11139. [PubMed: 15632174]

Moller CC, Wei C, Altintas MM, Li J, Greka A, Ohse T, Pippin JW, Rastaldi MP, Wawersik S, Schiavi S, Henger A, Kretzler M, Shankland SJ, Reiser J. Induction of TRPC6 channel in acquired forms of proteinuric kidney disease. J Am Soc Nephrol. 2007; 18:29–36. [PubMed: 17167110]

Mottl AK, Lu M, Fine CA, Weck KE. A novel TRPC6 mutation in a family with podocytopathy and clinical variability. BMC Nephrol. 2013; 14:104. [PubMed: 23663351]

Nilius B, Owsianik G. The transient receptor potential family of ion channels. Genome Biol. 2011; 12:218. [PubMed: 21401968]

Rastaldi MP, Armelloni S, Berra S, Calvaresi N, Corbelli A, Giardino LA, Li M, Wang GQ, Fornasieri A, Villa A, Heikkila E, Soliymani R, Boucherot A, Cohen CD, Kretzler M, Nitsche A, Ripamonti

M, Malgaroli A, Pesaresi M, Forloni GL, Schlondorff D, Holthofer H, D'AmicoG. Glomerular podocytes contain neuron-like functional synaptic vesicles. FASEB J. 2006; 20:976–978. [PubMed: 16585060]

Reiser J, Polu KR, Moller CC, Kenlan P, Altintas MM, Wei C, Faul C, Herbert S, Villegas I, Avila-Casado C, McGee M, Sugimoto H, Brown D, Kalluri R, Mundel P, Smith PL, Clapham DE, Pollak MR. TRPC6 is a glomerular slit diaphragm-associated channel required for normal renal function. Nat Genet. 2005; 37:739–744. [PubMed: 15924139]

Rohacs T. Regulation of transient receptor potential channels by the phospholipase C pathway. Adv Biol Regul. 2013; 53:341–355. [PubMed: 23916247]

Roshanravan H, Dryer SE. ATP acting through P2Y receptors causes activation of podocyte TRPC6 channels: role of podocin and reactive oxygen species. Am J Physiol Renal Physiol. 2014; 306:F1088–1097. [PubMed: 24553432]

Seifert JP, Wing MR, Snyder JT, Gershburg S, Sondek J, Harden TK. RhoA activates purified phospholipase C-epsilon by a guanine nucleotide-dependent mechanism. J Biol Chem. 2004; 279:47992–47997. [PubMed: 15322077]

Smrcka AV, Brown JH, Holz GG. Role of phospholipase Cepsilon in physiological phosphoinositide signaling networks. Cell Signal. 2012; 24:1333–1343. [PubMed: 22286105]

Taal MW, Brenner BM. Renoprotective benefits of RAS inhibition: From ACEI to angiotensin II antagonists. Kidney Int. 2000; 57:1803–1817. [PubMed: 10792600]

Vogt S, Grosse R, Schultz G, Offermanns S. Receptor-dependent RhoA activation in G12/G13-deficient cells: genetic evidence for an involvement of Gq/G11. J Biol Chem. 2003; 278:28743–28749. [PubMed: 12771155]

Wang H, Oestreich EA, Maekawa N, Bullard TA, Vikstrom KL, Dirksen RT, Kelley GG, Blaxall BC, Smrcka AV. Phospholipase C epsilon modulates beta-adrenergic receptor-dependent cardiac contraction and inhibits cardiac hypertrophy. Circ Res. 2005; 97:1305–1313. [PubMed: 16293787]

Weissmann N, Dietrich A, Fuchs B, Kalwa H, Ay M, Dumitrascu R, Olschewski A, Storch U, Mederos y, Schnitzler M, Ghofrani HA, Schermuly RT, Pinkenburg O, Seeger W, Grimminger F, Gudermann T. Classical transient receptor potential channel 6 (TRPC6) is essential for hypoxic pulmonary vasoconstriction and alveolar gas exchange. Proc Natl Acad Sci U S A. 2006; 103:19093–19098. [PubMed: 17142322]

Weissmann N, Sydykov A, Kalwa H, Storch U, Fuchs B, Mederos y, Schnitzler M, Brandes RP, Grimminger F, Meissner M, Freichel M, Offermanns S, Veit F, Pak O, Krause KH, Schermuly RT, Brewer AC, Schmidt HH, Seeger W, Shah AM, Gudermann T, Ghofrani HA, Dietrich A. Activation of TRPC6 channels is essential for lung ischaemia-reperfusion induced oedema in mice. Nat Commun. 2012; 3:649. [PubMed: 22337127]

Wettschureck N, Offermanns S. Mammalian G proteins and their cell type specific functions. Physiol Rev. 2005; 85:1159–1204. [PubMed: 16183910]

Winn MP, Conlon PJ, Lynn KL, Farrington MK, Creazzo T, Hawkins AF, Daskalakis N, Kwan SY, Ebersviller S, Burchette JL, Pericak-Vance MA, Howell DN, Vance JM, Rosenberg PB. A mutation in the TRPC6 cation channel causes familial focal segmental glomerulosclerosis. Science. 2005; 308:1801–1804. [PubMed: 15879175]

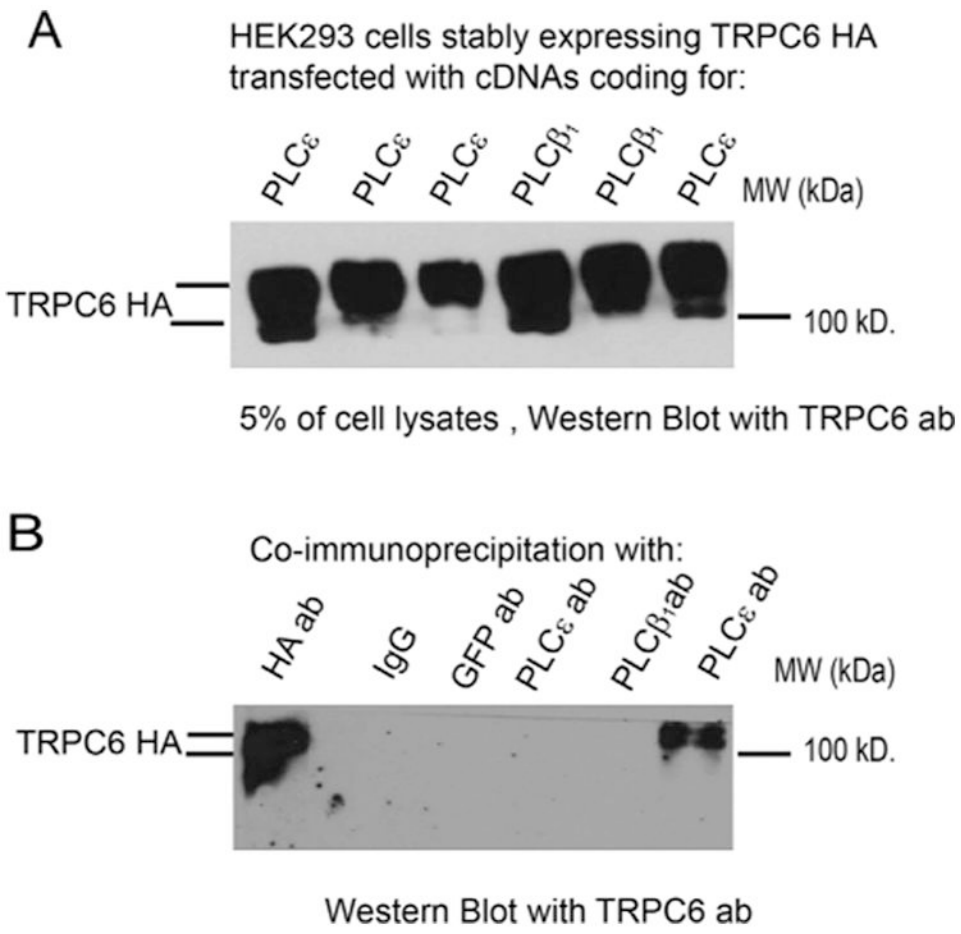

Fig. 1.

Co-immunoprecipitation of PLCε and TRPC6 heterologously expressed in HEK293 cells. (A) Immunoblots of proteins from lysates of HEK293 cells stably expressing hemagglutinin(HA)-tagged TRPC6 transfected with the indicated cDNAs before and (B) after co-immunoprecipitation with the indicated antibodies (upper panel). HA-tagged human TRPC6 is detected in both immunoblots by an HA specific antibody.

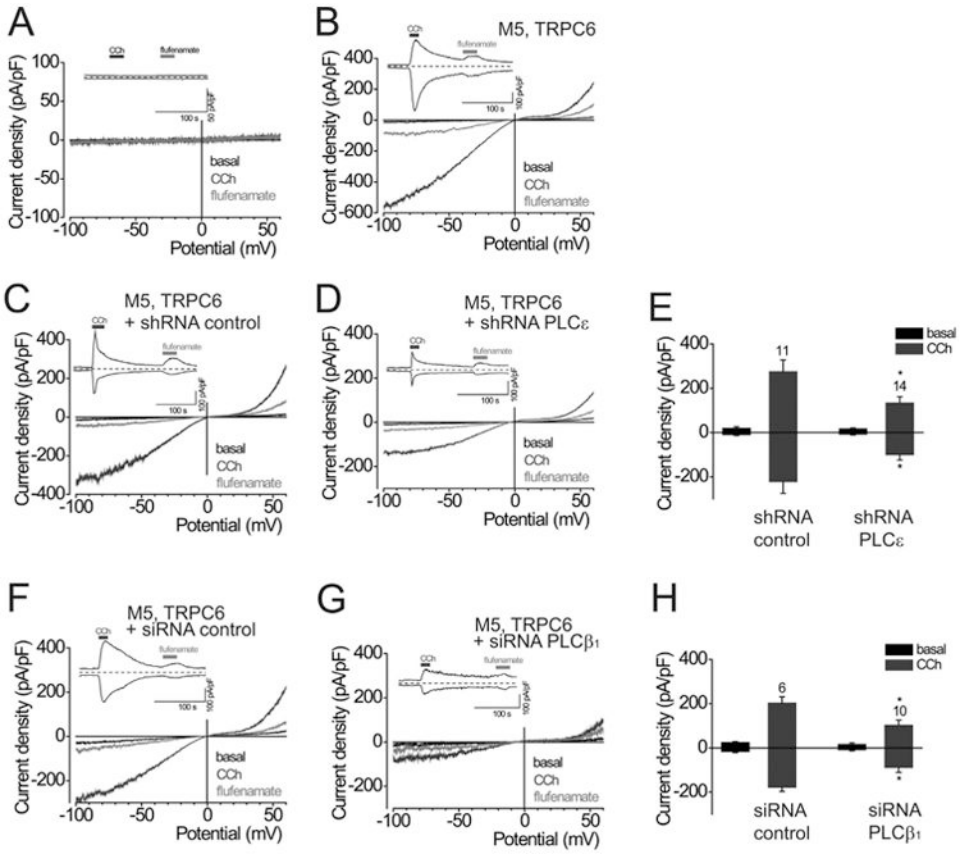

Fig. 2.

Electrophysiological analysis of PLCε TRPC6 interaction in HEK293 cells heterologously expressing TRPC6 (A–H). (A, B) Exemplary current density voltage relationships determined by patch-clamp recordings in the whole cell mode of non-transfected HEK293 cells (A) and of HEK293 cells transiently expressing muscarinic acetylcholine receptor 5 (M5) and TRPC6 (TRPC6) before (basal, black lines) and during receptor activation by carbachol (CCh, dark grey line) and during application of the TRPC6 activator flufenamte (flufenamate, grey lines). (C, D) Exemplary current density voltage relationships of TRPC6 currents in M5 and TRPC6 expressing HEK293 cells transfected with a scrambled small hairpin RNA (shRNA control, C) or a small hairpin RNA specific for PLCε (shRNA hPLCε, D) before and after application of carbachol or the TRPC6 activator flufenamate. (F, G) Current density voltage relationships of TRPC6 currents in M5 and TRPC6 expressing HEK293 cells transfected with a scrambled small interference RNA (siRNA control, F) or a small interference RNA specific for PLCβ_1 (siRNA hPLCβ_1, G) before and after application of carbachol or the TRPC6 activator flufenamate. A–D, F, G: *Insets* show current density time courses at ± 60mV. Applications of carbachol or flufenamate are indicated by bars. (E, H) Summary of current densities of shRNA hPLCε, siRNA hPLC β_1 -expressing or shRNA, siRNA control-expressing HEK293 cells analyzed by patch clamp recordings in the whole cell mode at ±60 mV before (black bars) and during (dark grey bars) application of carbachol. * and ** indicates significant differences $P < 0.05$ and 0.01, respectively.

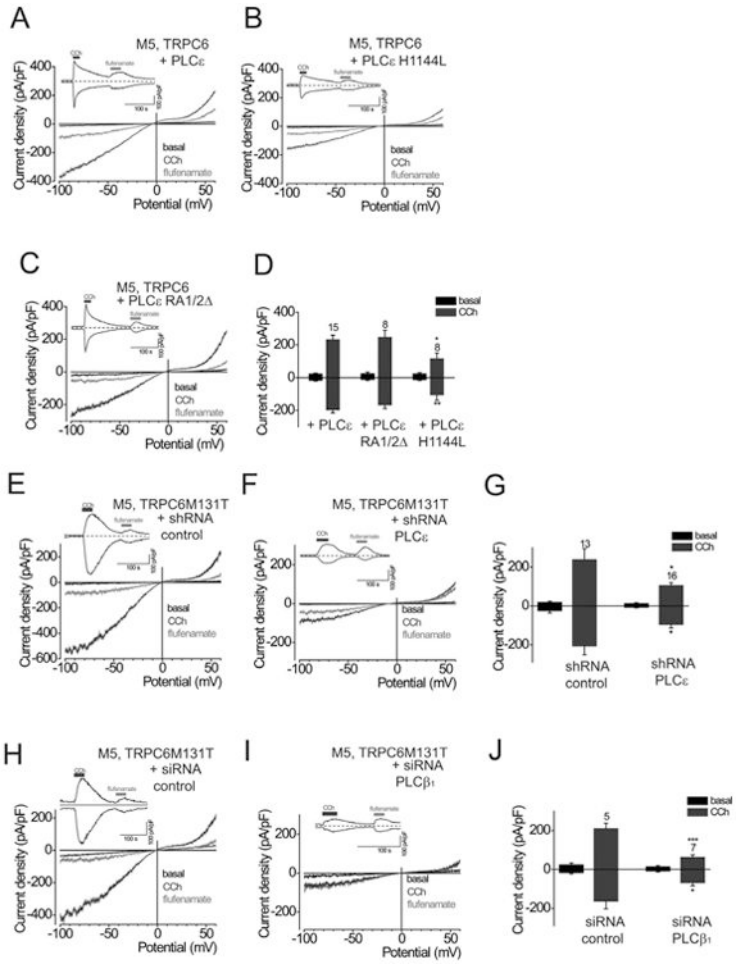

Fig. 3.

Electrophysiological analysis of PLCε and TRPC6 function in HEK293 cells (A–J). (A–C) Exemplary current-density voltage relationships determined by patch-clamp recordings in the whole cell mode in HEK 293 cells transiently expressing muscarinic acetylcholine receptor 5 (M5), TRPC6 (TRPC6) and PLCε (PLCε, A), a loss of function mutant of PLCε identified in FSGS patients (PLCε H1 144L, B) or a PLCε mutant with deleted Ras binding domains (PLCεRA1/2Δ, C) before (basal, black lines) and during application of the receptor agonist carbachol (CCh, dark grey line) or the TRPC6 activator flufenamte (flufenamate, grey lines). *Insets* show current density time courses at ± 60 mV of shRNA hPLCε/β_1-expressing or shRNA control-expressing HEK293 cells before and during application of carbachol or flufenamate. Applications of carbachol and flufenamte are indicated by bars. (D) Summary of current densities in HEK 293 cells expressing M5 receptor, TRPC6 and WT PLCε of mutant PLCε proteins at ± 60 mV before (black bars) and during (blue bars) application of carbachol. * and ** indicates significant differences $P < 0.05$ and 0.01, respectively. (E, F, H, I) Exemplary current-density voltage relationships in HEK 293 cells transiently expressing muscarinic acetylcholine receptor 5 (M5) and TRPC6M131T mutant together with scrambled small hairpin RNA (shRNA control, E), a small hairpin RNA specific for PLCε (shRNA hPLCε, F), a scrambled small interference RNA (siRNA control,

H) or a small interference RNA specific for PLCβ_1 (siRNA hPLCβ_1, I), before (basal, black lines) and during application of the receptor agonist carbachol (CCh, dark grey line) or the TRPC6 activator flufenamte (flufenamate, grey line). *Insets* show current density time courses at ± 60mV of shRNA hPLC$\varepsilon\beta_1$-expressing or shRNA control-expressing HEK293 cells before and during application of carbachol or flufenamate. Applications of carbachol and flufenamte are indicated by bars. (G, J) Summary of current densities of shRNA hPLCε, siRNA hPLCβ_1-co-expressing or shRNA, siRNA control-co-expressing HEK293 cells analyzed by patch clamp recordings in the whole cell mode at ± 60 mV before (black bars) and after (dark grey bars) application of carbachol. * and ** indicates significant differences $P < 0.05$ and 0.01, respectively.

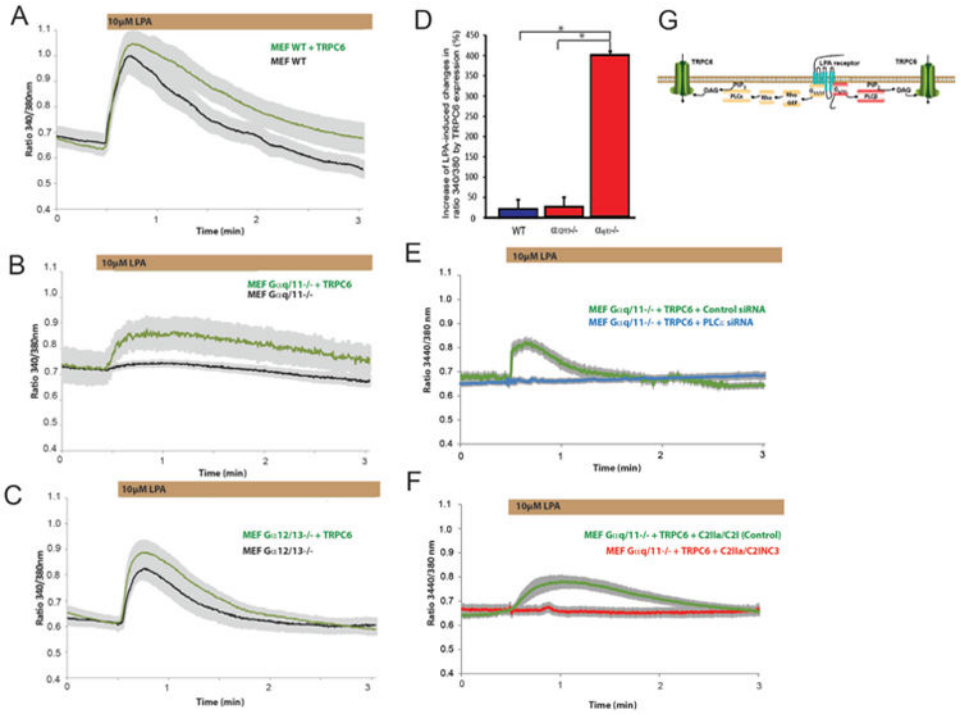

Fig. 4.

Analysis of intracellular Ca^{2+} $[Ca^{2+}]_i$ levels after stimulation of LPA receptors in wild-type $G_{\alpha q/11}$- or $G_{\alpha 12/13}$-deficient murine embryonic fibroblasts (MEFs) expressing TRPC6. (A) Wild-type (WT) MEF cells (MEF, WT, black trace) or WT MEF cells expressing TRPC6eGFP (MEF WT+TRPC6, green trace), (B) $G_{\alpha q/11}$-deficient MEFs (MEF Gαq11-/-, black trace) or $G_{\alpha q/11}$-deficient MEFs expressing TRPC6-eGFP (MEF Gαq11-/-+TRPC6, green trace) (C) $G_{\alpha 12/13}$-deficient MEFs (MEF Gα12/13-/-, black trace) or $G_{\alpha 12/13}$-deficient MEFs expressing TRPC6-eGFP (MEF Gα12/13-/-+TRPC6, green trace) were stimulated by lysophosphatidic acid (10 μM LPA) to induce receptor activated Ca^{2+} influx. Increases in $[Ca^{2+}]_i$ levels were detected by analysis of fluorescence ratios (Ratios 340/380 nm). The black and green lines represent calculated means, whereas the light gray areas indicate standard errors of the mean (S.E.M.). (D) Summary of increases of $[Ca^{2+}]_i$ levels in WT and TRPC6-expressing cells after receptor stimulation by LPA. (E) $G_{\alpha q/11}$-deficient MEFs expressing TRPC6-eGFP were transfected with a PLCε-specific (MEF Gαq11-/-+TRPC6+PLCε siRNA, blue trace) or control siRNA (MEF Gαq11-/-+TRPC6+control siRNA, blue trace) and (F) $G_{\alpha q/11}$-deficient MEFs expressing TRPC6eGFP were treated with Rho-inhibiting C2INC3+C2IIa (MEF Gαq11-/-+ TRPC6+Rho-inhibiting toxin, red trace) or for control with C2I+C2IIa (MEF Gαq11-/-+TRPC6+Control, green trace) were stimulated by lysophosphatidic acid (10 μM LPA) to induce receptor activated Ca^{2+} influx. Increases in $[Ca^{2+}]_i$ levels were detected by analysis of fluorescence ratios (Ratios 340/380 nm). (G) Summary of LPA receptor activated pathways inducing TRPC6 activation in MEF. The red, blue, and green lines represent calculated means, whereas the light gray areas indicate standard errors of the mean (S.E.M.). * indicates significant differences $P < 0.05$, respectively.

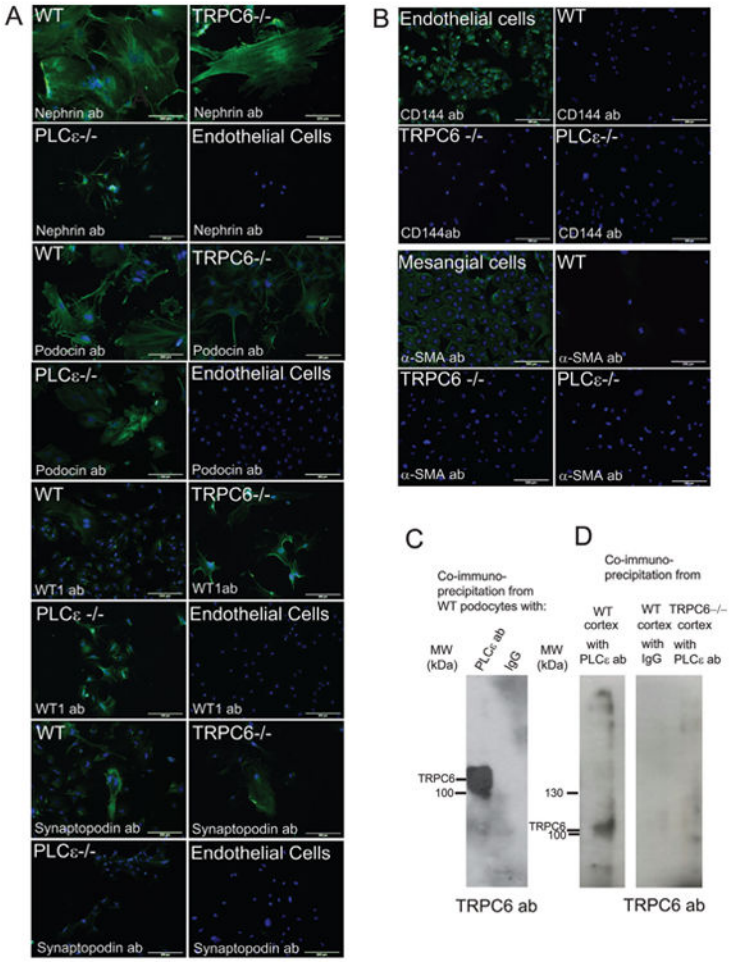

Fig. 5.

Immunohistochemical characterization of primary podocytes and co-immunoprecipitation of TRPC6 and PLCε in primary isolated podocytes and kidney cortex. (A) Primary isolated podocytes of three different genotypes (wildtype (WT), TRPC6-/- (TRPC6-/-) or PLCε-/- (PLCε-/-)) detected by a specific nephrin (Nephrin ab), podocin (Podocin ab), WT1 (WT1 ab) and synaptopodin (Synaptopodin ab) as well as a secondary antibody coupled to a fluorescence marker. (B) Primary isolated podocytes of three different genotypes (wildtype [WT], TRPC6-/-[TRPC6-/-] or PLCε-/- [PLCε-/-]) and endothelial (Endothelial cells) or mesangial cells (mesangial cells) were incubated with specific CD144 (CD144 ab) and α-smooth muscle actin (α-SMA) antibodies as well as a secondary antibody coupled to a fluorescence marker. (C) Immunoblot of protein lysates from co-immunoprecipitations of primary podocytes using a specific PLCε antibody (PLCε ab) or immunoglobulin g (IgG) incubated with a specific TRPC6 antibody (TRPC6 ab). (D) Immunoblot of protein lysates from co-immunoprecipitations of kidney cortex from WT and TRPC6-/- mice using a specific PLCε antibody (PLCε ab) incubated with a specific TRPC6 antibody (TRPC6 ab).

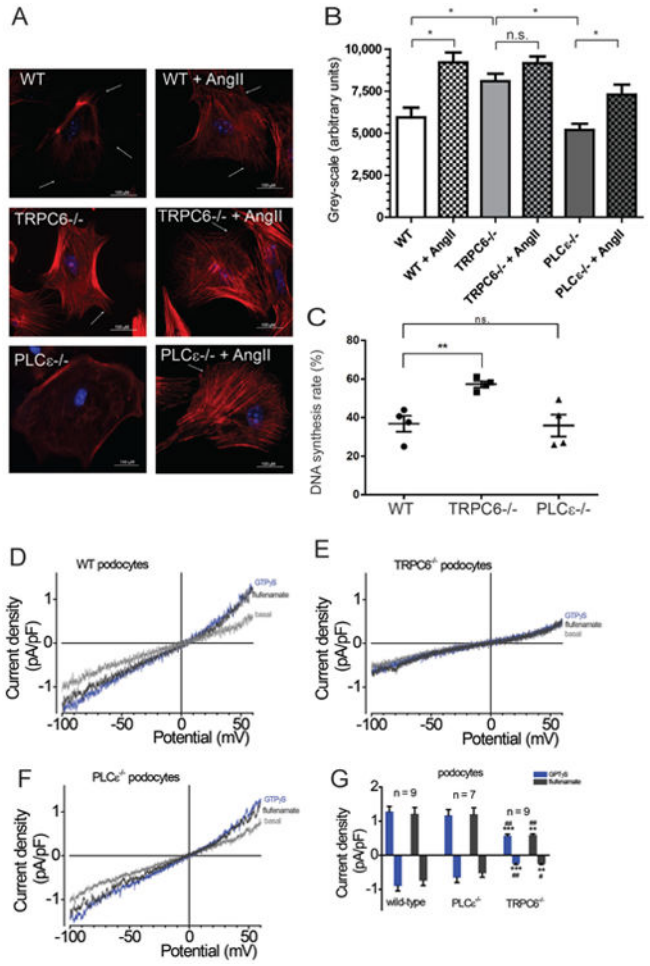

Fig. 6.

Actin stress fiber formation, DNA synthesis and GTPγS-induced currents in WT, TRPC6-/- and PLCε-/- podocytes. (A) Primary isolated podocytes of different genotypes were stained before and after incubation with angiotensin II (Ang II) with TRITC-labeled phalloidin to detect actin stress fibers. Arrows indicate cell borders. (B) Summary of actin stress fiber formation by quantification of relative grey values of TRITC phalloidin stained podocytes of different genotypes before and after adding angiotensin II (Ang II). (C) Quantification of DNA synthesis in podocytes of different genotypes using the EdU incorporation method. (D, E, F) GTPγS- and flufenamate-induced currents detected in podocytes of different genotypes by patch clamp recordings. Representative current-density voltage curves are shown. (G) Summary of current densities induced by GTPγS infusion or flufenamate application in podocytes of different genotypes at ± 60 mV. * and ** indicate significant differences $P<$ 0.05 and 0.01, respectively in A to F. In G * and ** indicate significant differences $P<0.05$ and 0.01 of TRPC6-/- podocytes compared to WT podocytes, while # and ## indicate significant differences $P < 0.05$ and 0.01 of TRPC6-/- podocytes compared to PLCε-/- podocytes.